# Optical nanoantennas applied to sensors

Jorge Diogo Dias Abrantes Farinha, 83384, MEEC

Instituto Superior Técnico, Academia Militar

e-mail: jorgefarinha92@gmail.com

**Abstract: In the last year nanotechnology has gained an ever increased importance in many areas from biology to engineering. In engineering, the development of nanometric devices and applications is on the agenda. Optical nanoantennas emerged has a fundamental device in the sensor field.**

**In this article, the behavior of optical aperture nano-antennas, a metal sheet with apertures of dimensions smaller than the wavelength, in a structure dielectric/metal/dielectric will be modelled and simulated. The modelling of this antennas requires the modeling of the electrical permittivity of the metal (gold) taking into account the plasmonic effects and the modelling of the diffraction of light when passing the apertures, namely in the Fresnel approximation. Diffraction theories for apertures with subwavelength dimensions, and the Rakic model for the electrical permittivity are introduced.**

**Simulation results were obtained using two different approaches, a numerical solution of the field equations using COMSOL Multiphysics and theoretical simulation of Fresnel diffraction using the program Mathematica.**

**Index terms: Nanotechnology, Optical antennas, near-field, diffraction pattern, superficial plasmon, extraordinary optical transmission.**

## I. Introduction

Antennas have been essential to establish communication between devices such as mobile phones, televisions, computers and generally in the telecommunication systems in the radio-frequency (RF) band. Optical antennas operate in the optical frequency band and are emerging as fundamental devices, not only in the usual communication applications, but also in other situations, for example to interact with molecules.

The accumulated knowledge about the antennas in the RF band has facilitated the development of optical antennas in the optical domain. In many cases, the structure of the antennas in the optical domain is analogous to those of RF (monopole, dipole, etc.) and the fundamental parameters that characterize an antenna are also important in optical antennas (gain, directivity, efficiency, etc). However the behavior of the optical antennas is dependent of new phenomena, such as the existence at the interface between metals and dielectrics of surface plasmon-polariton electromagnetic waves, which gives rise to resonant effects not available at RF. This phenomena are important to the appearance of the "extraordinary optical transmission" in metals, with a periodic set of apertures of dimensions smaller than the wavelength [1], [2].

In optical frequency band, optical antennas have applicability in many areas, such as physics, medicine, engineering, chemistry, and biology, among others. According to classical diffraction theories, the incident field is equal to the field at the apertures in the metal. But in the diffraction theory, for apertures with dimensions smaller than wavelength, the incident field is not equal to the field in the slit, as Bethe demonstrated and later Bouwkamp corrected, generalizing and correcting Bethe's theory [3], [4], [5].

The influence of the optical properties of metals on the electromagnetic wave propagation is considered through the definition of a complex electrical permittivity is dependent the electromagnetic wave frequency. In this case the permittivity model the Rakic model [6].

When a beam of light is incident on the metal with the apertures, the light is diffracted. The main objective in this work is the study of "near field", corresponding to the so-called Fresnel diffraction. In the following sections are presented some important analytical results, the simulations results using the program COMSOL Multiphysics® and the results of numerical simulation for rectangular slits, according the theory in Hecht [7] and Abedin [8], [9], [10].

## II. Optical Antennas

### A. Rakic Model

Optical properties of metals can be described by complex electrical permittivity which is dependent on the incident electromagnetic wave's frequency. This properties are determined by the fact that the conduction electrons can move freely within the bulk of material and that interband excitations can take place if the energy of the photons exceeds the band gap energy of the respective metal [12].

To characterize optical properties of metals it's used the Rakic model. This model takes into account two different models, the Drude-Lorentz and the Brendel-Bormann models to interpret both the free-electron and the interband part. Rakic, in [6], concluded that Brendel-Bormann model was better to describe properly the interband absorption in noble metals. This is due to the fact that this model reduces the errors generated by the Lorentz function.

Drude-Lorentz model contemplates the free-electrons contribution and the harmonic oscillations derivative of bound electrons. The electrical permittivity, according to Drude-Lorentz model, is given by [6]:

$$\varepsilon_{DL}(\omega) = \underbrace{\left[1 - \frac{f_0 \omega_p^2}{\omega\left(\omega - i\Gamma_0\right)}\right]}_{1} + \underbrace{\left[\sum_{j=1}^{k} \frac{f_j \omega_p^2}{\left(\omega_j^2 - \omega^2\right) + i\omega\Gamma_j}\right]}_{2} \quad (1)$$

In equation (1), the first component represents the Drude model, whose model represents the free-electrons effects and the second component represents the bound electrons effects and interband transitions. Equation (1) depends on the oscillator strength ($f_0$), the plasma frequency ($\omega_p$), the damping constant ($\Gamma_0$) and $k$ is the number of oscillators with frequency ($\omega_j$) and strength ($f_j$).

Brendel-Bormann model describes accurately interband absorption in noble metals, due to the use of a Gaussian function. So, Brendel-Bormann model has the same first component as equation 1, but a

different second component, where it's used Brendel-Bormann polynomial $\chi_j$. The electrical permittivity, according to Brendel-Bormann model, is given by [6]:

$$\varepsilon_{BB}(\omega) = \varepsilon_{\infty} - \frac{f_0 \omega_p^2}{\omega(\omega - i\Gamma_0)} + \sum_{j=1}^{k} \chi_j(\omega) \tag{2}$$

Where k is the number of Brendel-Bormann oscillators. The Brendel-Bormann polynomial is given by [6]:

$$\chi_j(\omega) = \frac{i\sqrt{\pi} f_j \omega_p^2}{2\sqrt{2} a_j \sigma_j} \left[ \omega\left( \frac{a_j - \omega_j}{\sqrt{2}\sigma_j} \right) + \omega\left( \frac{a_j + \omega_j}{\sqrt{2}\sigma_j} \right) \right] \tag{3}$$

From equation 3, $w(z) = e^{-iz^2} \cdot erfc(-iz)$, and where:

$$a_j = a_j' + i a_j'' = \frac{\omega}{\sqrt{2}} \left\{ \left[ 1 + \left( \frac{\Gamma_k}{\omega} \right)^2 \right]^{\frac{1}{2}} + 1 \right\}^{\frac{1}{2}} + i \frac{\omega}{\sqrt{2}} \left\{ \left[ 1 + \left( \frac{\Gamma_k}{\omega} \right)^2 \right]^{\frac{1}{2}} - 1 \right\}^{\frac{1}{2}} \tag{4}$$

In figure 1, it's compared the real component and imaginary component of electrical permittivity of the Drude-Lorentz model and the Brendel-Bormann model. The graphics, which were programmed in MATLAB and using values presented in [6], are the following:

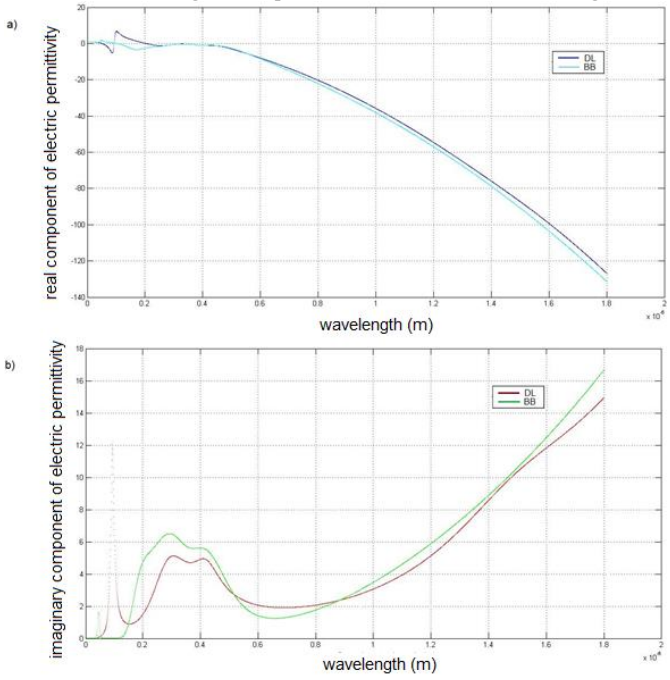


Fig. 1 – Graphic representation of the real component of electrical permittivity, a), and the imaginary component of electrical permittivity, b), using Rakic (DL) and Rakic (BB)

From figure 1, one sees that, for wavelength above ~0,3 $\mu m$, the real component of electrical permittivity is negative and decrease monotonously with the decrement of the wavelength. The imaginary component it's always positive and for $\lambda$>600nm it increases monotonously. One can observe, in fig.1 a), that the values of the different model values are rather close despite the values of B-B model being smaller to the values of D-L model. In fig. 1 b), the values of the different model values are rather close, but with smaller distinctions due to exhibit smaller scales. This graphics are the same as the one's programmed in [13].

The real component of electrical permittivity is related with storage of energy and reemission. The imaginary component is related with energy dissipation and absorption into the medium [14], [15].

The characterization of Rakic model, to describe the optical properties of metal, is fundamental to the existence of surface-plasmon-polariton electromagnetic waves at the dielectric/metal interface.

### *B. Surface plasmon- polariton*

The extraordinary optical transmission phenomenon is central for the applicability of optical antennas in sensors and biosensors. This phenomenon occurs due to surface plasmon-polariton in the dielectric/metal interface. Surface plasmons result from charge collective oscillation in the electron density at the surface of a metal. The interaction between plasmons and photons gives rise to plasmon-polariton that are surface electromagnetic waves, whose electromagnetic field is confined to the near vicinity of the dielectric-metal interface. This confinement leads to an enhancement of the electromagnetic field at the interface [11].

This enhancement of the electromagnetic field is denominated extraordinary optical transmission.

### *C. Extraordinary Optical Transmission*

In 1998, Ebbesen et al. observed that, when making focus a light beam in a thick metallic film, where there was a sub-wavelength hole array, occurs a large increase of incident electromagnetic wave transmission. This phenomenon is called extraordinary optical transmission [1].

Extraordinary optical transmission is an optical phenomenon, in which a structure containing subwavelength apertures transmits more light than might naively be expected. Such arrays may, for certain wavelengths, exhibit transmission efficiencies normalized to the total area of the holes that exceed unity. In other words, for these wavelengths a periodic array of subwavelength holes transmits more light than a large macroscopic hole with the same area as the sum of all the small holes. This phenomenon relies on the resonant excitation of surface plasmon-polariton at the metal–dielectric interface due to the periodicity of the sub-wavelength hole array. Extraordinary optical transmission is primarily due to constructive interference of SPPs propagating between the holes, where they can be coupled from/into radiation. The surprise is compounded by the fact that a single subwavelength aperture generally transmits light with an efficiency that is substantially below unity [1], [2], [16], [17], [18], [19], [20].

Bethe gave the first theory of diffraction by an idealized subwavelength aperture in a thin perfect metal layer, predicting extremely small transmitted powers as the aperture diameter decreased far below the radiation wavelength. These predictions were refuted by the observation of the so-called extraordinary optical transmission phenomenon by Ebbesen *et al.* [2].

### *D. Bethe and Bouwkamp theory*

The concern to describe the diffraction phenomenon through a sub- wavelength hole, took Bethe to develop a new diffraction theory of electromagnetic waves covering this situation. The theory was

applied to a circular hole in an ideal perfectly conducting and infinitely thin screen.

There are two major approximations in the Bethe-Bouwkamp theory of light transmission through a circular aperture in a screen. The screen is said to be made of an ideal perfectly conducting screen, and so perfectly opaque to the transmission of radiation, and its thickness is taken to be infinitely small. However, when discussing the transmission properties through real apertures, i.e., in real metals, the finite conductivity, and so the transmission, should be taken into account. The thin films used in optical experiments cannot be taken as perfectly opaque screens, and we could not employ the Bethe-Bouwkamp theory. On the other hand, if the film thickness is higher than some skin depths, that is, if we are dealing with a "thick" film, it could be taken as an opaque screen. It has been shown that for apertures fulfilling these conditions, localized surface plasmons have a significant influence in the transmission process [17].

The expressions that characterize the electromagnetic field in the hole region, according to Bethe model, are [4], [21]:

$$H_x = 0 \qquad H_y = \frac{1}{\mu_0 c} \qquad H_z = -\frac{4}{\mu_0 c \pi}\frac{y}{\sqrt{a^2 - x^2 - y^2}} \tag{5}$$

$$E_x = -\frac{4ik}{\pi}\sqrt{a^2 - x^2 - y^2} \qquad E_y = 0 \qquad E_z = ikx \tag{6}$$

In figure 2 is represented the total magnetic field deduced by Bethe, and in figure 3 is represented the total electric field deduced by Bethe , simulated using the program Mathematica by Gomes [22].

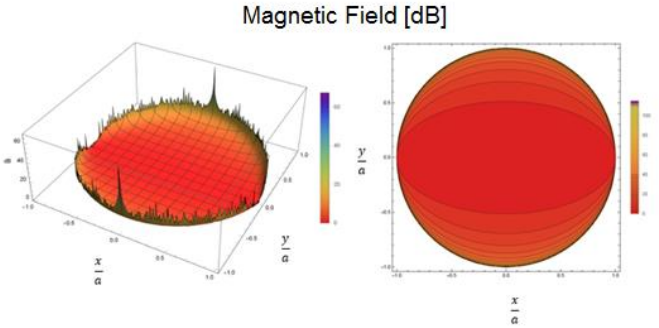


Fig. 2 – Total magnetic field in the aperture region, according to Bethe theory [22]

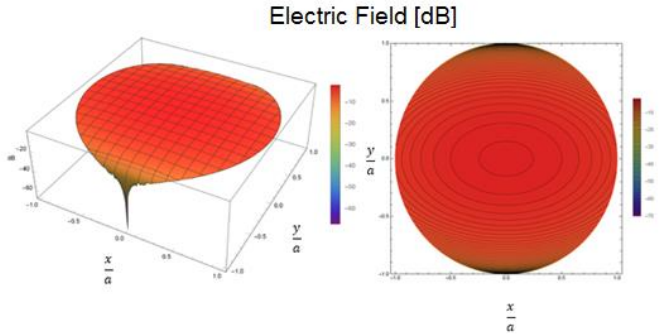


Fig. 3 - Total electric field in the aperture region, according to Bethe theory [22]

The result of Bethe it's not correct, since it implies that the electric field is discontinuous in the aperture, unlike what is required by the boundary conditions. From equation 6, the first order approximation of Bethe doesn't satisfy the condition $E_z = 0$ in the aperture [5].

Bouwkamp diffraction corrects and generalizes Bethe's theory, in particular in resetting the boundary conditions proposed by Bethe, which exhibit discontinuities and, in turn, do not serve as approximate solution to the problem of diffraction in the near field.

The expressions that characterize the electromagnetic field in the hole region, according to Bouwkamp model, are:

$$H_x = 0 \qquad H_y = 1 \qquad H_z = -\frac{4}{\pi}\frac{y}{\sqrt{a^2 - x^2 -}} \tag{7}$$

$$E_x = -\frac{4ik}{3\pi}\frac{2a^2 - x^2 -}{\sqrt{a^2 - x^2 -}} \qquad E_y = -\frac{4ik}{3\pi}\frac{xy}{\sqrt{a^2 - x^2 .}} \qquad E_z = 0 \tag{8}$$

In figure 4 is represented the total electric field according with Bouwkamp's corrections, simulated using the program Mathematica by Gomes [22].

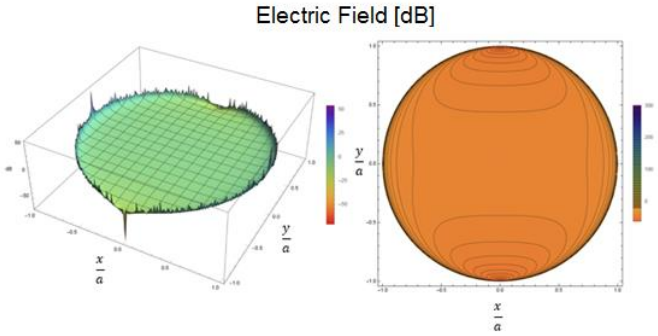


Fig. 4 - Total electric field in the aperture region, according to Bouwkamp theory [22]

The magnetic field deduced by Bowkamp doesn't change when compared to the one deduced by Bethe . From the observation of Fig. 3 and 4, one sees differences between the total electric field from the two theories. From Bethe's theory, the total electric field has his maximum value in the center of the hole and two minimums in the corners of the hole. From Bouwkamp's theory, the total electric field has his maximum and minimums values in the corners of the hole [4], [5], [21], [22].

### *E. Fresnel Diffraction*

The concept of diffraction was defined by Francesco Grimaldo, in 1600s, as a characteristic of wave phenomena occurring whenever a portion of a wave front, be it sound, a matter wave, or light, is obstructed in some way, that is, the deviation of light from rectilinear propagation. If after encountering an obstacle a region of the wave front is altered in amplitude or phase, diffraction will occur [7].

The study of diffraction pattern and irradiance in the near-field zone is denominated Fresnel diffraction.

The diffraction of light by a rectangular aperture is analyzed by Hecht [7] and Abedin [8]. Considering a simple rectangular aperture (Fig. 5), with an incident electromagnetic wave of wavelength λ emitted from a point source *S* is diffracted by a rectangular aperture of dimensions (*2a x 2b*). The right and left edges are located at $y_2$ and at $y_1$, respectively. The upper and lower edges are located ate $z_2$ and $z_1$, respectively. The diffracted light is observed on the screen positioned at a distance of $r_0$ from the aperture.

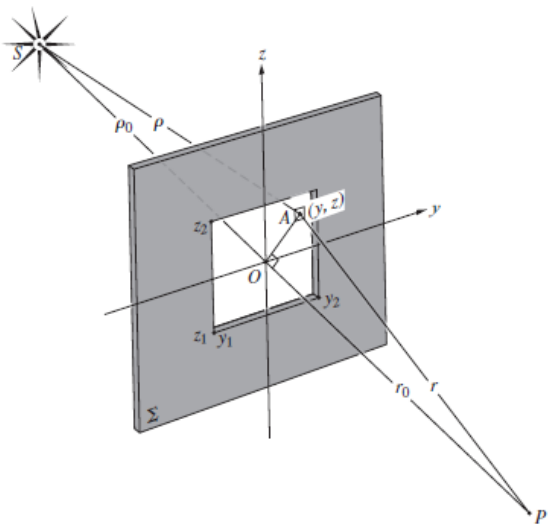


Fig. 5 – Fresnel diffraction for a rectangular aperture [7]

Being *P*, a point at the screen, the total electric field at *P* is given by [7], [8]:

$$\tilde{E}_P = \frac{\tilde{E}_u}{2}\left[C(u)+iS(u)\right]_{u_1}^{u_2}\left[C(v)+iS(v)\right]_{v_1}^{v_2} \tag{9}$$

Where *u* and *v* are dimensionless variables defined by [7], [8]:

$$u = y\left[\frac{2}{\lambda r_0}\right]^{\frac{1}{2}} \qquad v = z\left[\frac{2}{\lambda r_0}\right]^{\frac{1}{2}} \tag{10}$$

And $E_u$ is the unobstructed electric field at P, *C(w)* and *S(w)* are the Fresnel cosine and sine integrals and *w* represents either one of the two dimensionless variables *u* and *v*, respectively. The irradiance at *P* is given by $\frac{\tilde{E}_P\tilde{E}_P^*}{2}$, i.e. [7], [8]:

$$I_P = \frac{I_u}{4}\left\{\left[C(u_2)-C(u_1)\right]^2+\left[S(u_2)-S(u_1)\right]^2\right\}\times \left\{\left[C(v_2)-C(v_1)\right]^2+\left[S(v_2)-S(v_1)\right]^2\right\} \tag{11}$$

Where $I_u$ is the unobstructed irradiance corresponding to $E_u$.

Considering the case of a double aperture (Fig. 6), where the two edges of the right aperture are located at *y=a* and *y=b*, respectively, and the edges of the left aperture is located at *y=-a* and *y=-b*, respectively. The upper and lower edges are located at *z=c* and *z=-c*, respectively. The electric field at point P has two contributions, one from the right aperture and the other from the left aperture. The total electric field from the right aperture is given by [8]:

$$\tilde{E}_{PR} = \frac{\tilde{E}_u}{2}\left[C(u)+iS(u)\right]_{u_1}^{u_2}\left[C(v)+iS(v)\right]_{v_1}^{v_2} \tag{12}$$

Here the values of the limits $u_1$ and $u_2$ corresponds to the two edges of the right aperture, i.e. for $y_1=a$ and $y_2=b$, respectively. Similarly, the limits $v_1$ and $v_2$ corresponds to the lower and upper edges of this aperture, i.e. for $z_1=-c$ and $z_2=c$, respectively. The total electric field from the left aperture is given by [8]:

$$\tilde{E}_{PL} = \frac{\tilde{E}_u}{2}\left[C(u)+iS(u)\right]_{u_4}^{u_3}\left[C(v)+iS(v)\right]_{v_1}^{v_2} \tag{13}$$

Here the values of the limits $u_4$ and $u_3$ corresponds to the two edges of the left aperture, i.e. for $y_4=-b$ and $y_3=-a$, respectively. The values of the limits $v_1$ and $v_2$ are the same as in Eq. (12).

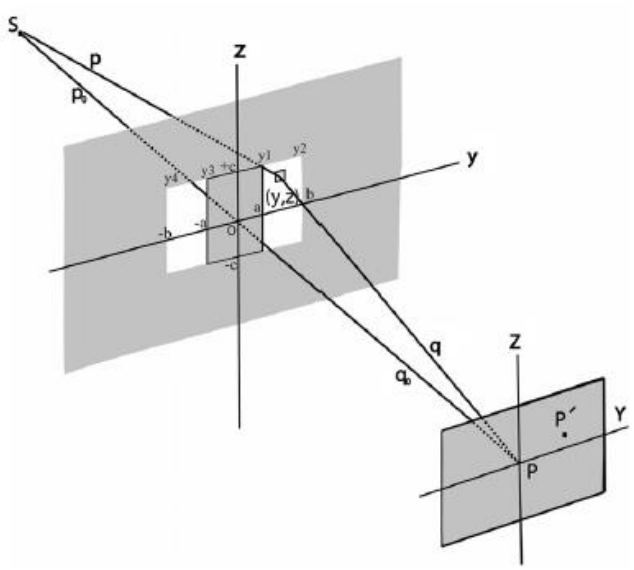


Fig. 6 – Fresnel diffraction for a double rectangular aperture [8]

The total electric field at P is the arithmetic sum of the two complex amplitudes from the left and right apertures, i.e.[8]:

$$\tilde{E}_P = \tilde{E}_{PE}+\tilde{E}_{PE} = \frac{\tilde{E}_u}{2}\left[\begin{array}{l}\left\{\begin{array}{l}C(u_2)+C(u_3)\\-C(u_1)-C(u_4)\end{array}\right\}\\+i\left\{\begin{array}{l}S(u_2)+S(u_3)\\-S(u_1)-S(u_4)\end{array}\right\}\end{array}\right] \times\left[\left\{C(v_2)-C(v_1)\right\}+i\left\{S(v_2)-S(v_1)\right\}\right] \tag{14}$$

The irradiance at P is given, the same way as in Eq. (11), by [8]:

$$I_P = \frac{I_u}{4}\left[\begin{array}{l}\left\{C(u_2)+C(u_3)-C(u_1)-C(u_4)\right\}^2\\+\left\{S(u_2)+S(u_3)-S(u_1)-S(u_4)\right\}^2\end{array}\right] \times\left[\left\{C(v_2)-C(v_1)\right\}^2+\left\{S(v_2)-S(v_1)\right\}^2\right] \tag{15}$$

Using the same procedure that was used to obtain equation (15), it's obtained the irradiance at P for four apertures, given by:

$$I_P = \frac{I_u}{4}\left\{\begin{array}{l}\left[\begin{array}{l}C(u_2)+C(u_4)+C(u_5)+C(u_7)\\-C(u_1)-C(u_3)-C(u_6)-C(u_8)\end{array}\right]^2+\\\left[\begin{array}{l}S(u_2)+S(u_4)+S(u_5)+S(u_7)\\-S(u_1)-S(u_3)-S(u_6)-S(u_8)\end{array}\right]^2\end{array}\right\} \times\left\{\left[C(v_2)-C(v_1)\right]^2+\left[S(v_2)-S(v_1)\right]^2\right\} \tag{16}$$

Here the edges of the first right aperture are $u_1$ and $u_2$, the edges of the second right aperture are $u_3$ and $u_4$, the edges of the first left aperture are $u_6$ and $u_5$ and the edges of the second left aperture are $u_8$ and $u_7$. The values of the limits $v_1$ and $v_2$ are the same as in Eq. (16).

Equation 16 is going to be used in Mathematica simulations in order to compare the simulation results obtained using COMSOL Multiphysics® for a four apertures nanoantenna.

## III. Numerical Results

In this section, a set of simulations are going to be presented. First is going to be presented the theoretical simulations using the program Mathematica. Second is going to be presented the simulations modeling the problem using program COMSOL Multiphysics® which uses the finite element method. The simulations results from Mathematica are used to confirm the simulations results from COMSOL Multiphysics®. For the simulations, in COMSOL Multiphysics®, were used a wavelength of the incident electromagnetic wave of λ=1550 nm. This wavelength represents a photon energy of ħω≈0.8 e.V, with a normalized Planck constant of $\hbar = 6.582 \times 10^{-16}\ eV \cdot s$. The signal source is at a distance of 10λ from the optical nanoantenna with four slits. The structure where the signal source is focused is a dielectric/metal/dielectric with dimensions of 10λ of length and 20λ of width. The dielectric used is the air. The metal used is the gold with 300nm of thickness. The metal it's characterized by the Rakic model (B-B), that is, with complex electrical permittivity of $-96.957 + i \cdot 11.504$. The four apertures have three variations of width and three variations of gap width between apertures, 2λ, λ and λ/10. The graphics represents irradiance over space and time. In COMSOL Multiphysics®, irradiance is represented as the square of the total electric field normalized to the incident electric field, whose value is $E_0=10^{-6}$ V/m, i.e., $|E/E_0|^2$. The results from the simulations are obtained, in Fresnel region, at a distance of 0.0967 μm from the aperture.

Considering a 2D aperture, the dimensionless variables $v_1$ and $v_2$ are infinite. Knowing that $C(\infty) = S(\infty) = 0.5$ and $C(-\infty) = S(-\infty) = -0.5$, we can use this approximation in Eq. (12) and obtain:

$$I_P = \frac{I_u}{2}\left\{\begin{bmatrix} C(u_2)+C(u_4)+C(u_5)+C(u_7) \\ -C(u_1)-C(u_3)-C(u_6)-C(u_8) \end{bmatrix}^2 + \begin{bmatrix} S(u_2)+S(u_4)+S(u_5)+S(u_7) \\ -S(u_1)-S(u_3)-S(u_6)-S(u_8) \end{bmatrix}^2\right\} \quad (17)$$

Eq. (17) was used in program Mathematica to obtain the theoretical results of the diffraction pattern and irradiance.

The simulation results for a four apertures array obtained from Mathematica are:

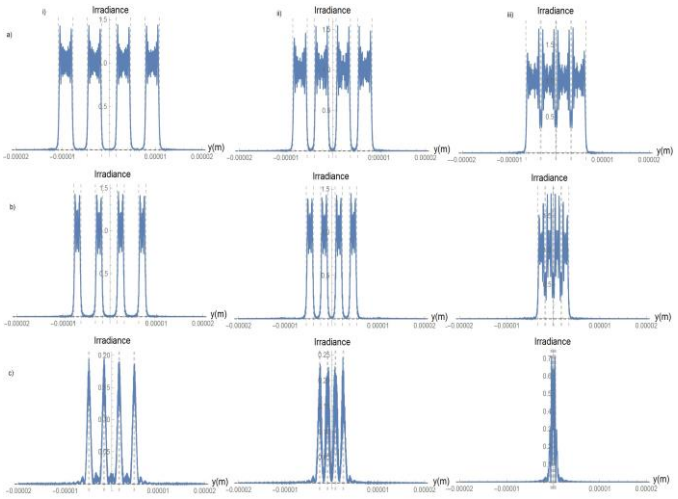


Fig. 7 – Simulation results for a four apertures array obtained using Mathematica with dimension of a) 2λ, b) λ and c) λ/10 and with gap spacing of i) 2λ, ii) λ and iii) λ/10

The grey lines in Fig. 7 represent the aperture dimensions.

It has used an automatic extremely thin mesh in COMSOL Multiphysics®. The following parameters that control the mesh element size are [23]:

**Maximum element size**: To limit the allowed element size, for example, if you want to limit the maximum element size to a fraction of the wavelength to make sure that the wave propagation is fully resolved.

**Minimum element size**: To specify the minimum allowed element size. You can use this value to, for example, prevent the generation of many elements around small curved parts of the geometry.

**Maximum element growth rate**: To determine the maximum rate at which the element size can grow from a region with small elements to a region with larger elements. The value must be greater or equal to one. For example, with a maximum element growth rate of 1.5, the element size can grow by at most 50% (approximately) from one element to another.

**Curvature factor**: To determine the size of boundary elements compared to the curvature of the geometric boundary (it is the ratio between the element size and the radius of curvature). The curvature radius multiplied by the curvature factor, which must be a positive scalar, gives the maximum allowed element size along the boundary. A smaller curvature factor gives a finer mesh along curved boundaries.

**Resolution of narrow regions**: To control the number of layers of elements that are created in narrow regions (approximately). The value must be a nonnegative scalar. A higher value gives a finer mesh in narrow regions. If the value of this parameter is less than one, the mesh generator might create elements that are anisotropic in size in narrow regions.

So it was used the following mesh parameters:

Maximum element size: 0.31 μm;

Minimum element size: 6.2e-4 μm;

Maximum element growth rate: 1.1;

Curvature factor: 0.2;

Resolution of narrow regions: 1.

The simulation results for a four apertures array obtained from COMSOL Multiphysics® are:

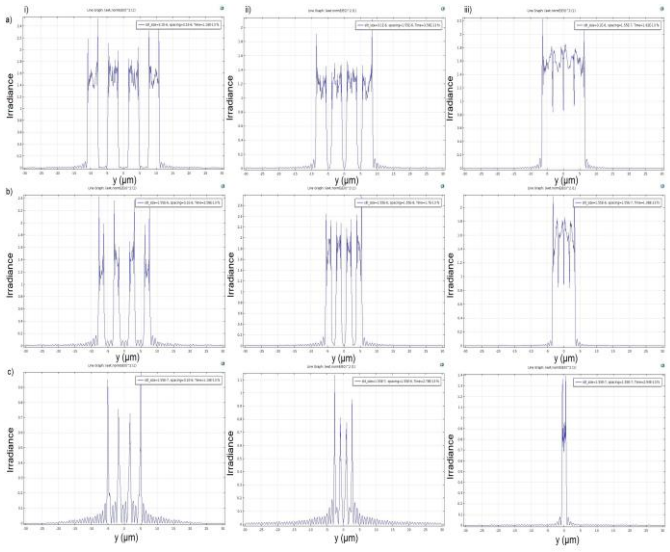

Fig. 8 - Simulation results for a four apertures array using COMSOL Multiphysics® with dimension of a) 2λ, b) λ and c) λ/10 and with gap spacing of i) 2λ, ii) λ and iii) λ/10

From Fig. 7 and 8 we can observe the diffraction pattern. The simulation results for a four apertures array, the maximum of irradiance, obtained from Fig.7 and Fig. 8 are the following:

| Aperture dimension | Gap spacing | Maximum Irradiance for Fresnel Diffraction | Maximum Irradiance for Rakic model |
|---|---|---|---|
| $2\lambda$ | $2\lambda$ | 1.40 | 2.50 |
| | $\lambda$ | 1.55 | 2.10 |
| | $\lambda/10$ | 1.70 | 2.20 |
| $\lambda$ | $2\lambda$ | 1.45 | 2.40 |
| | $\lambda$ | 1.45 | 2.70 |
| | $\lambda/10$ | 1.80 | 2.10 |
| $\lambda/10$ | $2\lambda$ | 0.20 | 1.00 |
| | $\lambda$ | 0.24 | 1.15 |
| | $\lambda/10$ | 0.70 | 1.40 |

Table 1- Maximum irradiance from the simulations

From the observation of fig.7 and fig.8, that represent the obtained results, respectively, in Mathematica and COMSOL programs, one can verify that the diffraction patterns are identical for all the nine combinations between aperture width and gap width. For this case, one observes a diffraction pattern image similar to the antenna draw. The transmission peaks match with the aperture location. The irradiance maximum values (table 1) are very similar, with the values from Mathematica simulations (fig. 7) smaller than the values from COMSOL simulations (fig. 8). These differences are due to numerical errors derivate from the COMSOL mesh creation, due the optical phenomena not taking account in Fresnel diffraction and due to irradiance numerical errors given by the Fresnel diffraction. One can observe, in table 1, the occurrence of extraordinary optical transmission for all the combinations.

## IV. 3D SIMULATIONS

After the 2D simulations with an automatic extremely thin mesh in COMSOL Multiphysics®, it was simulated a 3D dielectric/metal/dielectric structure with dimensions of 20λ of length plus 300 nm of metal thickness, 20λ of width and height. It was used only one aperture with 10λ of width and λ/10 of height. The gold was characterized by the Rakic model (B-B), that is, with complex electrical permittivity of $-96.957 + i \cdot 11.504$.. This 3D simulation was done with an automatic coarse mesh, with means that will be errors in the values of the irradiance due to a big mesh, because it was the one that could run because with a more dense mesh there were more points to calculate and needed more computer RAM. This mesh is characterized by a maximum element size of 4.65 μm, minimum element size of 0.868 μm, maximum element growth rate of 1.6, curvature factor of 0.7 and resolution of narrow regions of 0.4. The incident electric field $E_0$ used in COMSOL Multiphysics® was $10^{-6}$ V/m . The irradiance is characterized by total electric field $E$ normalized to the incident electric field, $|E/E_0|^2$. This normalization allows to verify if the radiation that passed through the hole is bigger or smaller than 1 and verifying, or not, the existence of extraordinary optical transmission. The results from the simulations are obtained, in Fresnel region, at a distance of 1.40 μm from the aperture.

The 3D simulation result for a one aperture obtained from COMSOL Multiphysics® for the near-field is:

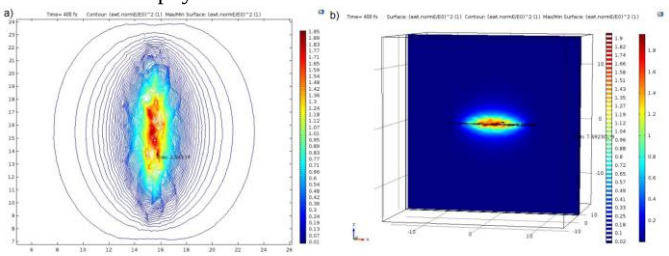

Fig. 9 – 3D simulation results for an optical antenna with one aperture obtained with COMSOL Multiphysics®, for the near-field, obtained a) in a 2D plan and b) in a 3D plan

From Fig.9, it was obtained, from the 3D simulations results from COMSOL Multiphysics® for an optical antenna with one aperture, in the near-field, a maximum irradiance value of 2.34534.

## V. RESULT'S DISCUSSION

From Fig.7 and 8 we can observe the similarity between the diffraction patterns of the Mathematica simulations using Eq. (17) and the COMSOL Multiphysics® simulations. This means that Fresnel diffraction it's very accurate giving the diffraction pattern.

Regarding the maximum irradiance, the differences between the values are due numerical errors occurring in the automatic mesh creation by COMSOL Multiphysics®, the appearance of surface plasmon-polariton and the optical properties of metals. This means that Fresnel diffraction doesn't include this phenomena that only occur in optical regime where interaction between light-matter matters. We can observe that the sub-wavelength aperture is worst comparing the other two aperture dimensions, meaning that in some way, there is interference in the wave that leaves to an irradiance decrease. Nevertheless, from all the results, we are towards extraordinary optical transmission. So the best result, from the COMSOL Multiphysics® simulations, is the one in grey in table 1.

From Fig.9, in the 3D simulations with a coarse mesh it was observed extraordinary optical transmission. Being these results obtained with a big mesh in COMSOL Multiphysics®, it is expected to have numerical errors in the irradiance calculation in this program. With these results, Bethe-Bouwkamp diffraction theory is not valid for subwavelength hole arrays.

## VI. CONCLUSIONS

In this work we simulated aperture antennas with four apertures. The electrical permittivity of the metal was modelled through the Rakic model. Variations on the gap spacing among apertures and on the aperture dimensions were considered.

The analyzed structure was the one showing the best results.

With the results presented previously, it was obtained more electric field in the near-field zone than the incident electric field,

meaning that we are towards extraordinary optical transmission discovered by Ebbesen *et al.* in sub-wavelength hole arrays in nanometric optical antennas in the optical band, which are very important in the future when using sensors and biosensors, among others devices from the various fields.

## REFERENCES


[1] T. W. Ebbesen *et al.*, "Extraordinary optical transmission through sub-wavelength hole arrays," *Nature*, vol. 86, no. 6, pp. 1114–7, 1998.

[2] M. Agio, *Optical antennas*. Cambridge University Press, 2013.

[3] P. Bharadwaj, B. Deutsch, and L. Novotny, "Optical Antennas," *Adv. Opt. Photon.*, vol. 1, p. 438, 2009.

[4] H. A. Bethe, "Theory of diffraction by small holes," *Phys. Rev.*, vol. 66, no. 7–8, pp. 163–182, 1944.

[5] C. J. Bouwkamp, "Diffraction Theory," *Reports Progresses Phys.*, vol. 17, pp. 35–100, 1954.

[6] A. D. Rakic, A. B. Djurisic, J. M. Elazar, and M. L. Majewski, "Optical properties of metallic films for vertical-cavity optoelectronic devices.," *Appl. Opt.*, vol. 37, no. 22, pp. 5271–5283, 1998.

[7] E. Hecht, *Optics*, 5th editio. Pearson, 2017.

[8] K. M. Abedin and S. M. M. Rahman, "Computer simulation of Fresnel diffraction from double rectangular apertures in one and two dimensions using the iterative Fresnel integrals method," *Opt. Laser Technol.*, vol. 44, no. 2, pp. 394–402, 2012.

[9] K. M. Abedin and S. M. Mujibur Rahman, "The iterative Fresnel integrals method for Fresnel diffraction from tilted rectangular apertures: Theory and simulations," *Opt. Laser Technol.*, vol. 44, no. 4, pp. 939–947, 2012.

[10] K. M. Abedin and S. M. M. Rahman, "Fresnel diffraction from N-apertures: Computer simulation by iterative Fresnel integrals method," *Optik (Stuttg).*, vol. 126, no. 23, pp. 3743–3751, 2015.

[11] A. V. Zayats, I. I. Smolyaninov, and A. A. Maradudin, "Nano-optics of surface plasmon polaritons," *Phys. Rep.*, vol. 408, no. 3–4, pp. 131–314, 2005.

[12] L. (University of R. Novotny and B. U. of B. Hecht, *Principles of Nano-Optics*, vol. 1, no. 4. 2006.

[13] A. Webster, "Complex Permittivity and Refractive Index for Metals," no. 5, pp. 1–13, 2012.

[14] J. D. Jackson, "Jackson - Classical Electrodynamics (3rd Ed.).pdf," *American Journal of Physics*. p. 641, 1962.

[15] M. Mahbuba, N. A. Chisty, and A. I. University-bangladesh, "Study of the Relative Permittivity Response of Metal Nanoantenna at Optical Frequency," vol. 5013, no. 3, pp. 584–587, 2014.

[16] V. A. G. Rivera, F. A. Ferri, O. B. Silva, F. W. A. Sobreira, and E. M. Jr., "Light Transmission via Subwavelength Apertures in Metallic Thin Films," in *Plasmonics - Principles and Applications*, Intech, 2012, pp. 157–182.

[17] K. Y. Kim, *Plasmonics - principles and applications*. InTech.

[18] B. Hou and W. Wen, "Enhanced Transmission of Acoustic Waves Through Subwavelength Holes in Hard Plates," 2013.

[19] S. G. Rodrigo, *Optical properties of nanostructured metallic systems*. 2012.

[20] F. J. Garcia-Vidal, L. Martin-Moreno, T. W. Ebbesen, and L. Kuipers, "Light passing through subwavelength apertures," *Rev. Mod. Phys.*, vol. 82, no. 1, pp. 729–787, 2010.

[21] A. M. Marino and G. Piredda, "Diffraction by a Small Circular Aperture," pp. 1–6.

[22] R. Gomes, "Estudo de uma antena ótica para comunicação inter- satélites," 2016.

[23] COMSOL Multiphysics, *Comsol Multiphysics Reference Manual*. 2013.


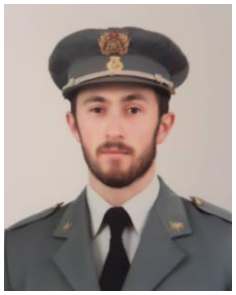


**Jorge Farinha** was born in Lisbon, Portugal on June 29, 1993.
In 2011, he joined the Portuguese Army where he completed his degree in electrotechnical engineering at Military Academy, in Lisbon. At the same time, he is a Master Student in Electrical and Computer Engineering Master Course at Instituto Superior Técnico.